



## Elevated temperature effects on local buckling of wide flange columns

Nikki Baidar<sup>1</sup>, Rachel Chicchi<sup>2</sup>

### Abstract

Steel wide flange columns under compression, which are adequately designed for ambient conditions, may fail through local buckling when subjected to fire conditions. This is because the sections may behave as slender elements at elevated temperatures due to strength and stiffness reductions in the mechanical properties of the steel. The AISC *Specification* (2016) does not currently provide provisions for determining local buckling capacity of columns under fire. This work aims to build on previous studies to determine the local buckling capacity of columns under uniaxial compression at elevated temperature. Numerical models of wide flange steel columns under fire conditions were developed using the finite element modelling software, ABAQUS. A parametric study of steel stub columns subjected to different temperatures (ambient, 400°C, and 600°C) and various section slenderness ratios was conducted. The failure load determined from the modeling for each of the steel columns was compared with the load capacity calculated using the current AISC equation for local buckling at ambient temperature with material properties corresponding to elevated temperature. It was found that the current AISC equations are inadequate to predict the local buckling capacity of column with slender elements at elevated temperature. Some sections that failed through global buckling at ambient temperature failed through local buckling at elevated temperatures.

### 1. Introduction

Fire can cause irreparable damage to columns, which can cause the collapse of the structure or failure to perform under service conditions. Fire causes strength and stiffness reductions of steel members, which alter the load carrying capacity of the columns designed at ambient conditions. Columns under compression, which are adequately designed for ambient conditions, may fail through local buckling when subjected to the fire conditions. Under elevated temperatures, the steel properties used to design the column at room temperature degrade, such as modulus of elasticity ( $E$ ), yield strength ( $F_y$ ), and ultimate strength ( $F_u$ ) (AISC 360-16, 2016). Because of this, the member may fail at a much lower load than what it was originally designed for, due to the reduced member capacity under elevated temperature.

In an I-shaped member, the flange is considered to be slender if the ratio  $b/t > 0.56 \sqrt{E/F_y}$ , where  $b$  is half of the flange width,  $t$  is the thickness of flange,  $E$  is the modulus of elasticity,  $F_y$  is the

---

<sup>1</sup> Graduate Research Assistant, University of Cincinnati, <baidarni@mail.uc.edu>

<sup>2</sup> Assistant Professor, University of Cincinnati, <chicchrl@ucmail.uc.edu>

yield strength. For a web to be slender, the ratio  $h/t_w > 1.49 \sqrt{E/F_y}$  where  $h$  is the clear distance between the flanges and  $t_w$  is the thickness of the web. At ambient temperature, when the cross-section is not slender, the global buckling controls the failure mode of column. When the elements are slender, column strength is calculated by implementing the effective area approach, which is based on the reduced effective widths of the flanges and web.

Cross-sectional slenderness, which can cause local buckling, is controlled by limiting the element (flange or web) width to thickness ratio to maintain nonslender elements. However, these limiting ratios may change at elevated temperatures because they are affected by material stiffness ( $E$ ) and strength ( $F_y$ ).

The effect of local buckling at ambient temperature is addressed and well presented in the AISC *Specification*, but AISC does not currently present any design provisions to account for the effect of local buckling under elevated temperatures (AISC 360-16, 2016). Research is needed to determine if the same equations used for design at ambient temperature can also be valid at elevated temperature or fire design. This lack of design equations for local buckling under fire load has motivated this research.

### *1.1 Literature review*

Yang et al. (2006) studied H steel columns under elevated temperature and examined the effects of width to thickness ratio and slenderness on causing either local buckling or global buckling through experimental testing. In their experiment, the columns that failed from global buckling under ambient temperature failed from local buckling under elevated temperature. When temperature exceeded 500°C, reduction in strength was noted with columns retaining only 70% of their ambient strength when the slenderness ratio ( $L/r$ ) was less than 50, where  $L$  is the laterally unbraced length of the member and  $r$  is the radius of gyration. A significant drop in strength was noted when slenderness ratios were greater than 50. The study suggested that a critical temperature of 500°C should be adopted to retain two-thirds of the ambient temperature yield strength and a slenderness ratio of 50 should be adopted to prevent brittle failure.

Seif and McAllister (2013) used the temperature approach in which the column is evaluated under a fixed gravity load while the temperature is increased. For applied loads up to 40% of their yield capacity, the element slenderness did not affect the temperature at which members buckled significantly. But, when the applied loads reached greater than 60% of their yield capacity, the columns with slender flanges buckled at increasingly lower temperatures. Only when long columns were loaded at 80% of their yield capacity, length played a role in determining the temperature at which the sections buckled.

Wang et al.(2014) performed an experimental study on welded H stub columns with simultaneous application of axial load and temperature. Buckling resistance of the flanges and web was studied separately for both room and elevated temperatures. For the same width-to-thickness ratio or height-to-thickness ratio, the buckling load of the column decreased as the temperature increased. The strength degradation of 50% and 80% was observed in the columns at 450°C and 650°C, respectively. Between 450°C and 650° C, rapid decrease in both strength and stiffness of columns occurs. They also reported that in comparison to mild steel (Q235), high strength steel (Q460) columns are more susceptible to local buckling at elevated temperature.

## 2. Numerical Modelling

The finite element method (FEM) modeling used to simulate the local buckling behavior of steel at elevated temperature is presented in this section.

### 2.1 Model description

A 3D deformable thin shell element was used to model the column in ABAQUS, a finite element modelling software. Linear quadrilateral elements of type S4R were used to perform the buckling analysis. A S4R is a 4-node doubly curved shell element. A global mesh size 5 mm, which was determined from benchmarked studies, was used to mesh the entire model. Pinned-pinned boundary conditions were used in the numerical model for the parametric study.

Initial imperfections were introduced using the mode shape obtained from linear buckling analysis. Mode 1 was selected, which showed deformations in the flanges and web that were similar to local imperfections. The benchmarking method adopted by Wang et al. (2014) for their numerical model used the magnitude of local imperfections as 1% of the plate thickness or  $0.01t$ , where  $t$  is the thickness of the specimen, based on recommendations in Chen & Young (2008). Global buckling was not considered as an initial imperfection in this study.

The residual stress of rolled shapes at elevated temperatures is not well defined. For this reason, the residual stress having a linear distribution with maximum residual stress being  $0.3F_y$  as recommended in the *AISC Specification* was first applied in the model (AISC 360-16, 2016). Residual stresses were applied using the method outlined in Akhtar and Chicchi (2021). Second, the model was constructed without the application of residual stress. No notable differences to the peak capacity were observed between the two models at elevated temperature. Thus, the residual stress was not used in the model. Yang et al. (2006) also found that residual stress does not seem to contribute to the ultimate load at elevated temperature conditions. The generic material properties corresponding to each temperature, 20°C, 400°C, and 600°C, were applied using Eurocode 3 (2005).

### 2.2 Modelling procedure

First, a linear buckling analysis was performed to develop initial imperfections in the column, which was applied to the nonlinear buckling model. The result of the linear buckling analysis provides the different mode shapes and corresponding eigenvalues. Fig. 1 shows the flange and web imperfection for the section.

A nonlinear buckling analysis was performed implementing the dynamic explicit method in which the compressive load was gradually increased until the column failed at a certain elevated temperature. The uniform temperature was first applied to the column and then the axial load was applied. The nonlinear material properties of ASTM A992 steel (Gr. 50) at 400°C and 600°C were applied in the column to simulate material behavior at elevated temperature. A sample result of a nonlinear buckling analysis is shown in Fig. 2.

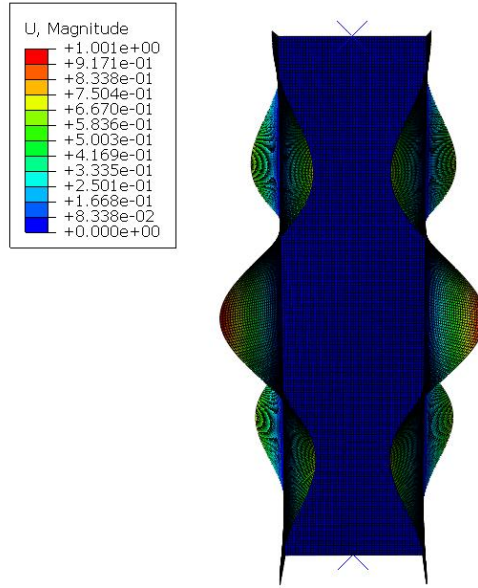


Figure 1: Local imperfection obtained as result from linear buckling analysis

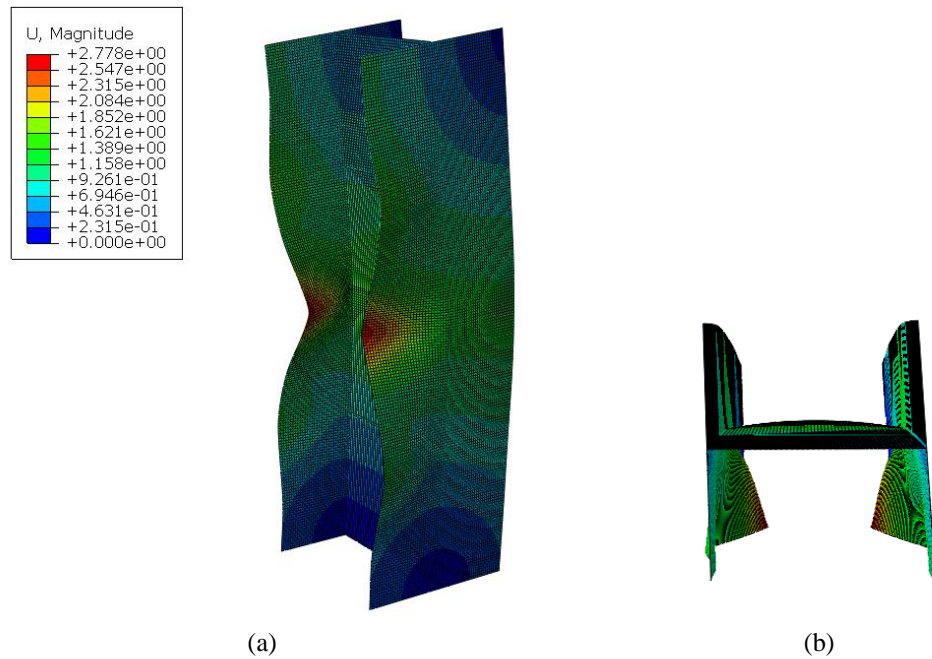


Figure 2: Local buckling obtained as result from nonlinear buckling analysis a) Isometric view and b) Plan view

## 2.2 Validation of numerical model

Two different I-section stub columns were modelled from the Wang et al. (2014) experimental work. The specimens had a length of 70 inches and was subjected to uniaxial compression at an elevated temperature. This experiment was replicated analytically, implementing the modelling approach described above. In the experiment, the temperature was increased in the columns until it reached the elevated temperature, 450°C or 650°C, and then the axial load was applied. Table 1

provides a comparison between the results from the experiment by Wang et al. (2014) and the results obtained from the finite element model.  $P_{EXP}$  represents the results obtained during experimental testing by Wang et al. (2014).  $P_{FEM}$  represents the benchmarked results obtained in ABAQUS to validate the modeling approach. It can be seen that the modeling approach implemented in this study does a reasonable job of estimating the ultimate capacity of the columns.

Table 1: Column capacity determined by experiment and FEM

Section	Temperature	Section size, inch <sup>1</sup>	Ultimate load, kips		
			$P_{EXP}$	$P_{FEM}$	$P_{EXP}/P_{FEM}$
Q235A	650°C	9.84×9.84×0.24×0.31	66.3	73.1	0.91
Q235A	450°C	9.84×9.84×0.24×0.31	209	196.5	1.06
Q235B	650°C	12.44×7.87×0.24×0.31	62.94	69.24	0.91

<sup>1</sup>The sizes are depth × width ×  $t_w$  ×  $t_f$  in inches.

#### 4. Parametric study

After the validation of the numerical modelling procedure, different stub columns of 40 inches length were modelled for the parametric study, which helped to identify the influence of different slenderness parameters on the steel column under fire conditions. This study focuses on wide flange columns using ASTM A992 steel (Gr. 50) steel. Load carrying capacity was evaluated for these columns to study the effect of elevated temperature on local buckling under varied parameters of the numerical model. The effects of slenderness of the cross-section (flange and web) and the applied elevated temperature on local buckling was investigated. Each of the columns were modelled at three different temperatures: 20°C, 400°C and 600°C. Ambient temperature is presumed to be at 20°C.

The three different steel cross-sections studied were W14×120, W12×96, and W10×88. These are common wide flange steel column sections used in the US that have different depths and that are not overly heavy. These sections are not slender at ambient temperature but may become slender at elevated temperature. Column sizes that have slender elements at ambient temperature are rarely ever used, which is why non-slender cross-sections were selected instead. Each of these original three sizes were modified to encompass a range of  $b/t$  and  $h/t_w$  ratios. In order to do this, the column width and height were kept constant, but the flange and web thicknesses were varied. Table 2 shows the sections that were used in the parametric study and their sizes. Section A in each series is the original column size. Sections B through J represent modifications to the original section. A section designated as W12-A means that the W12×96 shape was used with the original, unmodified section. W12-J, for instance, means that the original W12×96 shape was modified according to the dimensions for name J in Table 2. The flange limiting ratio for ASTM A992 steel at ambient conditions is 13.48 and the web limiting ratio is 35.88.

For each section, thickness was varied for both the flange and the web. Each section was analyzed with the following cross-sectional properties: slender flange and non-slender web, slender flange and slender web, non-slender flange and slender web, and non-slender flange and non-slender web according to ambient temperature, as can be seen in Fig. 3. The dashed lines in the figure represents the distinction between a slender and non-slender element for both the web and the flange.

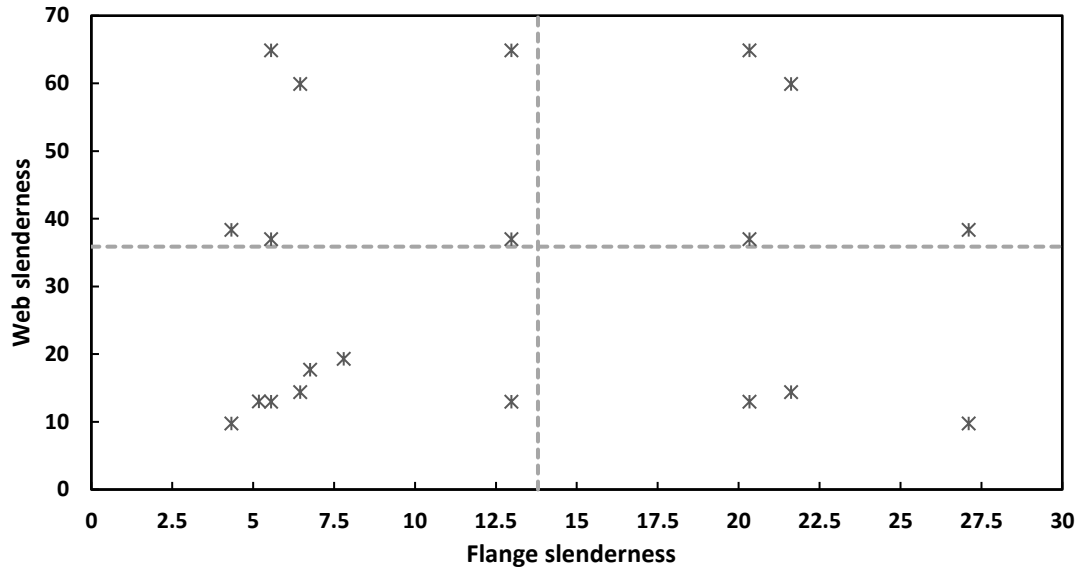


Figure 3: Web and flange slenderness of each column selected for parametric study

Table 2: Section and their sizes used in the parametric study

Cross-section	Name	Flange				Web			
		$b$ , in	$t_f$ , in	Width to thickness ratio ( $b/2t_f$ )	Slender/Nonslender	$h$ , in	$t_w$ , in	Height to thickness ratio ( $h/t_w$ )	Slender/Nonslender
W12×96	A	12.2	0.9	6.76	Nonslender	9.74	0.55	17.70	Nonslender
	B	12.2	1.1	5.55	Nonslender	9.74	0.75	12.98	Nonslender
	C	12.2	0.3	20.33	Slender	9.74	0.15	64.90	Slender
	D	12.2	1.1	5.55	Nonslender	9.74	0.15	64.90	Slender
	E	12.2	0.3	20.33	Slender	9.74	0.75	12.98	Nonslender
	F	12.2	1.1	5.55	Nonslender	9.74	0.26	37.00	Slender
	G	12.2	0.3	20.33	Slender	9.74	0.26	37.00	Slender
	H	12.2	0.47	12.98	Nonslender	9.74	0.75	12.98	Nonslender
	I	12.2	0.47	12.98	Nonslender	9.74	0.15	64.90	Slender
	J	12.2	0.47	12.98	Nonslender	9.74	0.26	37.00	Slender
W14×120	A	14.7	0.94	7.80	Nonslender	11.39	0.59	19.30	Nonslender
	B	14.7	1.14	6.45	Nonslender	11.39	0.79	14.41	Nonslender
	C	14.7	0.34	21.62	Slender	11.39	0.19	59.93	Slender
	D	14.7	1.14	6.45	Nonslender	11.39	0.19	59.93	Slender
	E	14.7	0.34	21.62	Slender	11.39	0.79	14.41	Nonslender
W10×88	A	10.3	0.99	5.18	Nonslender	7.87	0.61	13.00	Nonslender
	B	10.3	1.19	4.33	Nonslender	7.87	0.81	9.77	Nonslender
	C	10.3	0.19	27.11	Slender	7.87	0.21	38.37	Slender
	D	10.3	1.19	4.33	Nonslender	7.87	0.21	38.37	Slender
	E	10.3	0.19	27.11	Slender	7.87	0.81	9.77	Nonslender

## 5. Results and discussion

Fig. 4, Fig. 5 and Fig. 6 show the effect of slenderness at elevated temperature. Fig. 4 is a comparison of the section W12-A and the sections W12-E, W12-G, and W12-J at ambient temperature. The force applied to the column ( $P_u$ ) is normalized by the gross cross-sectional area ( $A_g$ ) of each shape in order to more directly compare the force-displacement relationships of the columns. The displacement is the vertical displacement at the top of the column as load is being applied. Section W12-A failed through global buckling while the other sections that have slender elements (W12-E, W12-G, and W12-J) failed through local buckling at ambient temperature. W12-G had both a slender web and slender flanges and it reached a  $P_u/A_g$  ratio much lesser than the other shapes. W12-E had a slender flange and a nonslender web, while W12-J had nonslender flanges and a slender web. The peak  $P_u/A_g$  ratios for these shapes were comparable.

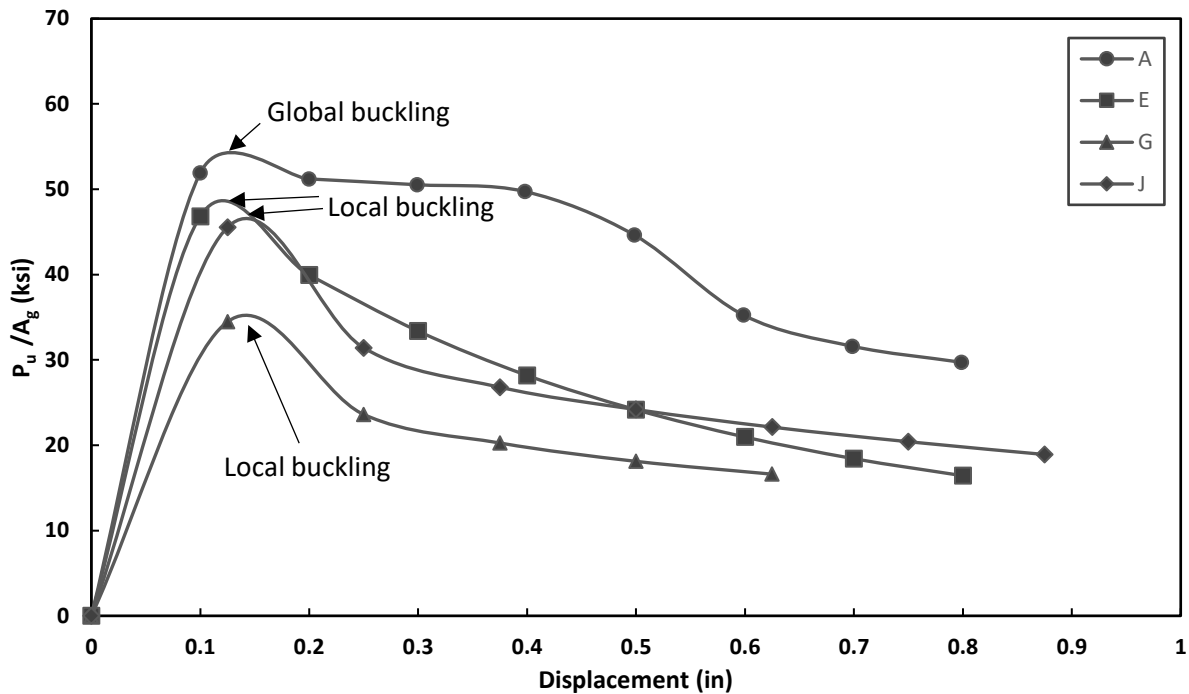


Figure 4:  $P_u/A_g$  vs. displacement plot for W12×96 column at ambient temperature with varied web and flange slenderness ratio

Fig. 5 is a comparison of the original section W12-A and the sections W12-E, W12-G, and W12-J at 400°C. These four sections failed through local buckling at 400°C. Again, the  $P_u/A_g$  ratio and axial displacements determined from ABAQUS are presented. When comparing with the ambient case from Fig. 4, it is evident that there is a softening effect occurring in the force-displacement response due to the reduced elastic modulus at 400°C. The peak  $P_u/A_g$  ratios for each section are also reduced.

From Fig. 5, in the case of W12-A and W12-E, strain hardening occurred and with an increase in strain, the stress ( $P_u/A_g$ ) also increased. When the sections W12-A and W12-E reached their ultimate strength, they failed through local buckling. At 400°C, sections W12-G and W12-J failed at a lower uniform stress ( $P_u/A_g$ ) and much lesser displacement than sections W12-A and W12-E.

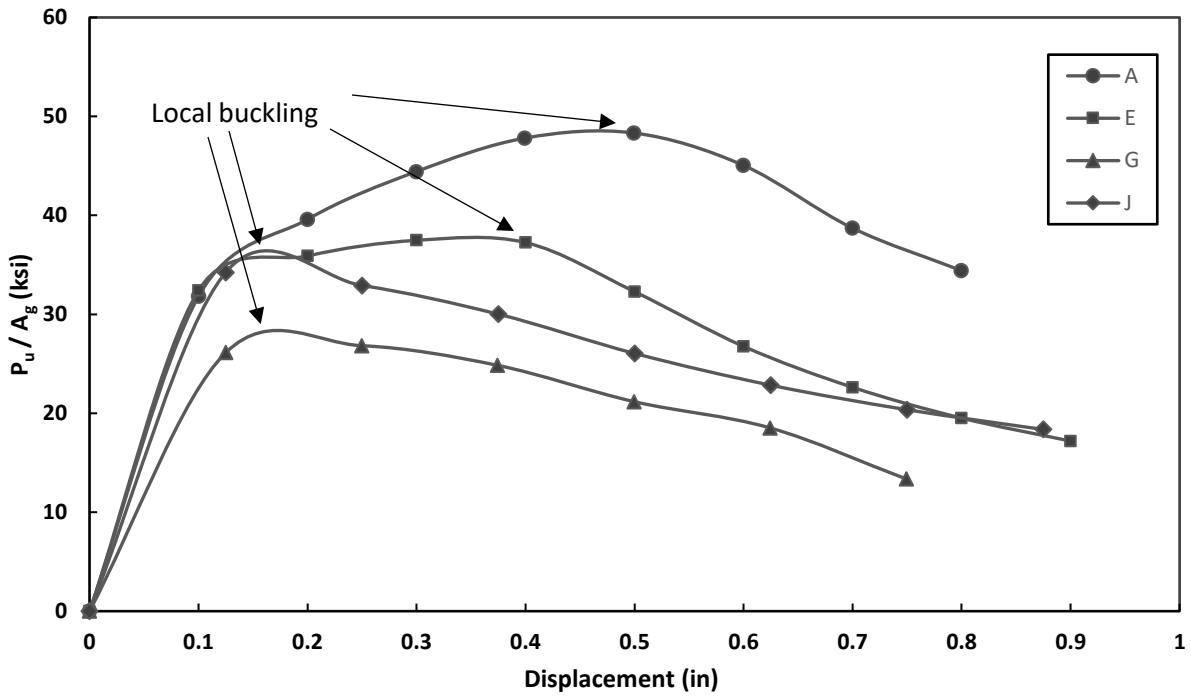


Figure 5:  $P_u/A_g$  vs displacement plot for W12×96 column 400°C with varied web and flange slenderness ratio

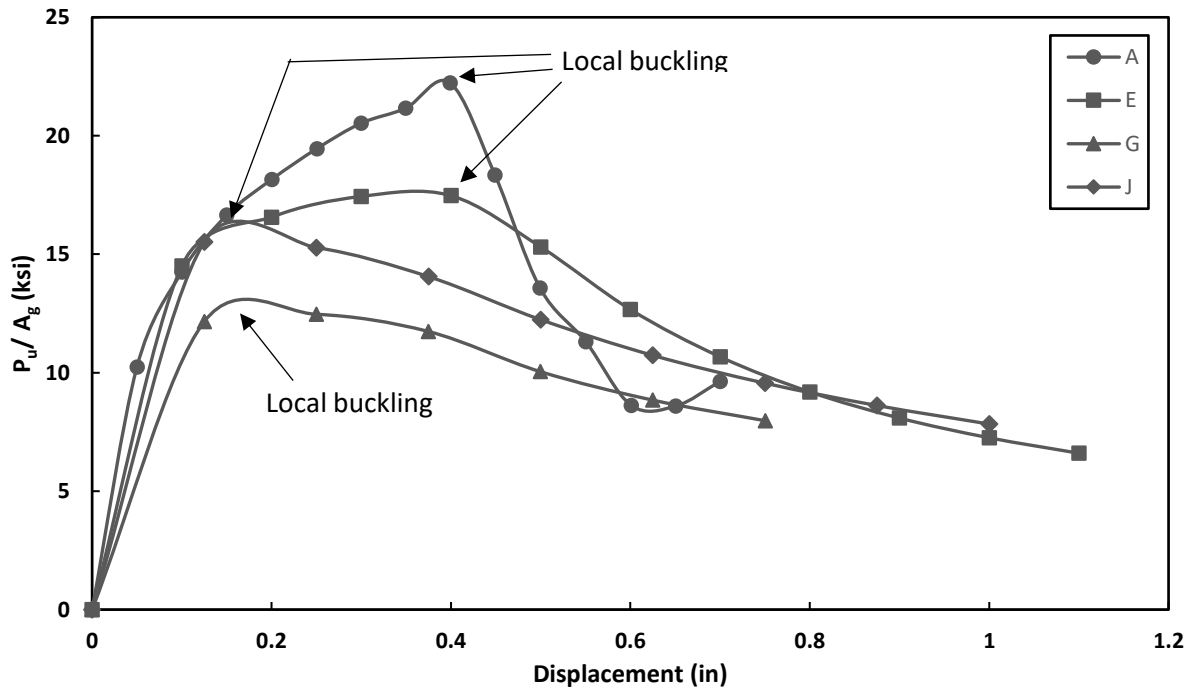


Figure 6:  $P_u/A_g$  vs. displacement plot for W12×96 column 600°C with varied web and flange slenderness ratio

Fig. 6 is a comparison of the column W12-A and column W12-E, W12-G, and W12-J at 600°C. From Fig. 5 and Fig. 6, similar behavior was observed for all four columns at 400°C and 600°C

with all sections failing in local buckling. However, these columns failed at significantly lower average stress than in the case of 400°C.

In the case of column W12-A and W12-E, there is decrease in stress ( $P_u/A_g$ ) and increase in displacement corresponding to the ultimate load at 400°C and 600°C when compared to the ambient temperature results. When comparing the three sections W12-E, W12-G and W12-J; section W12-E is the least slender and it failed through local buckling and had the highest buckling capacity among the three. Sections W12-G and W12-J that are too slender, failed through local buckling at all three temperatures before any material yielding.

The ultimate load capacities obtained from the finite element analyses performed in ABAQUS are presented in Table 3. Strength degradations determined by comparing ambient to 400°C tests show a mean degradation of approximately 10%. Strength degradations determined by comparing ambient to 600°C tests show a mean degradation of approximately 58%. Thus, the effects of local buckling on column at 400°C are minor relative to 600°C, which produces significant strength reductions that must be considered.

Table 3: Load capacities obtained from FEM analyses

Section		Slenderness		Load Capacity from FEM (kips)		
		Flange	Web	Ambient	400°C	600°C
W12×96	A	Nonslender	Nonslender	1417.8*	1320.2	607.4
	B	Nonslender	Nonslender	1798.1*	1812.6*	855.2*
	C	Slender	Slender	257.1	206.5	95.7
	D	Nonslender	Slender	1394.2	1387.6	651.9
	E	Slender	Nonslender	684.9	548.1	255.5
	F	Nonslender	Slender	1453.1	1397.3	671.8
W14×120	G	Slender	Slender	339.6	264.3	122.8
	H	Nonslender	Nonslender	994.9	841.5	392.6
	I	Nonslender	Slender	562.4	415.9	192.2
	J	Nonslender	Slender	637.6	479.4	217.2
	A	Nonslender	Nonslender	1785.6*	1737.0	813.2
	B	Nonslender	Nonslender	2221.5*	2247.8*	1045.1*
W10×88	C	Slender	Slender	329.8	285.4	134.6
	D	Nonslender	Slender	1758.9	1754.9	835.4
	E	Slender	Nonslender	813.5	707.6	329.1
	A	Nonslender	Nonslender	1317.9*	1313.5*	607.8*
	B	Nonslender	Nonslender	1633.3*	1568.6*	766.5*
W10×88	C	Slender	Slender	156.1	132.8	62.4
	D	Nonslender	Slender	1302.0	1293.5	601.6
	E	Slender	Nonslender	479.4	360.1	170.9

\*Indicates that the sections failed through global buckling at that temperature.

### 5.1 Local buckling capacity calculated using AISC equation vs. obtained using FEM

The load capacity of the steel columns at elevated temperature obtained from the numerical model results was compared with the load capacity calculated using the current AISC equation for local buckling. The result of this comparison is provided in Fig. 7 for both ambient and elevated temperature.

In Fig. 7, the y-axis consists of the normalized load which is  $P_u/P_n$ , where  $P_u$  is the maximum load capacity obtained from ABAQUS and  $P_n$  is the nominal compressive strength calculated using Eq. 1:

$$P_n = F_{cr}A_e \quad (1)$$

Where,  $F_{cr}$  is the critical stress calculated from Section E3 of the *AISC Specification* (AISC 360-16, 2016) and  $A_e$  is the summation of effective areas of the cross-section based on reduced effective widths,  $b_e$  (flange) or  $h_e$  (web) calculated from Section E7 of the *AISC Specification* which is used for slender sections. Section E7 of the *AISC Specification*, which calculates the capacity of slender section for the ambient temperature, was used but with mechanical properties of yield strength and modulus of elasticity that correspond with each temperature. Table 4 shows the temperature dependent material properties of ASTM A992 steel.  $E(T)$  is the modulus of elasticity of the material when subjected to temperature,  $T$ . It is calculated by multiplying the modulus of elasticity at ambient by the reduction factor for each temperature provided in Appendix 4 (AISC 360-16, 2016).  $F_y(T)$  is the yield strength of the material when subjected to temperature,  $T$ . It is calculated by multiplying the yield strength at ambient by the reduction factor for each temperature provided in Appendix 4 (AISC 360-16, 2016).

Table 4: Temperature dependent material properties of ASTM A992 steel

Temperature, T	E(T), ksi	F <sub>y</sub> (T), ksi
20°C	29000	50
400°C	20356	50
600°C	9887	24.5

These values were used to calculate the effective width of each slender column, which provides the column capacity at ambient temperature, 400°C and 600°C. The x-axis in Fig. 7 consists of the interactive slenderness  $(\lambda_f/\lambda_{rf})(\lambda_w/\lambda_{rw})$ , where  $\lambda_f$  is the flange slenderness of the column,  $\lambda_w$  is the web slenderness of the column,  $\lambda_{rf}$  is the limiting slenderness ratio of the flange at ambient temperature, and  $\lambda_{rw}$  is the limiting slenderness ratio of the web at ambient temperature.

The sloped trendline was drawn for 600°C temperature results, which shows a decreasing strength ratio ( $P_u/P_n$ ) as the interactive slenderness increases. This decreasing trend was observed at all three temperatures. The horizontal dashed line represents a normalized load of 1.0, which means that the AISC provisions predict the load capacity well for the column at that temperature. A load ratio greater than 1.0 means that the AISC provisions are conservative, while values less than 1.0 indicate that the provisions are not conservative, and use of an alternative equation ought to be considered.

From Fig. 7, in the ambient temperature case, the columns with an interactive slenderness less than 1.0 (meaning these are stockier columns), have their results better predicted using the AISC

provisions and their normalized load is approximately 1 to 1.1. The columns with slenderness less than 0.55, which are original sections and sections stockier than original section, mostly failed through global buckling in case of the ambient temperature. The columns with slenderness greater than 1.5 (highly slender elements) resulted in non-conservative estimates of column capacity with normalized load values around 0.8 to 0.85.

From Fig. 7, elevated temperature cases 400°C and 600°C, show a similar decreasing pattern. In the case of 400°C, for columns with the interactive slenderness less than 1.0, the normalized load is calculated to be around 1.1 to 0.9. As the interactive slenderness increases from 0.55 onwards, the normalized load was determined to be 0.89 to 0.73 and local buckling was the controlling failure mode.

There is a slight change in slope of the results at 600°C when compared to 400°C. In the case of 600°C, for columns with interactive slenderness less than 1, the normalized load was approximately 1.1 to 0.78. As the slenderness increased from 0.55 onwards, the normalized load was 0.86 to 0.53 and local buckling was observed.

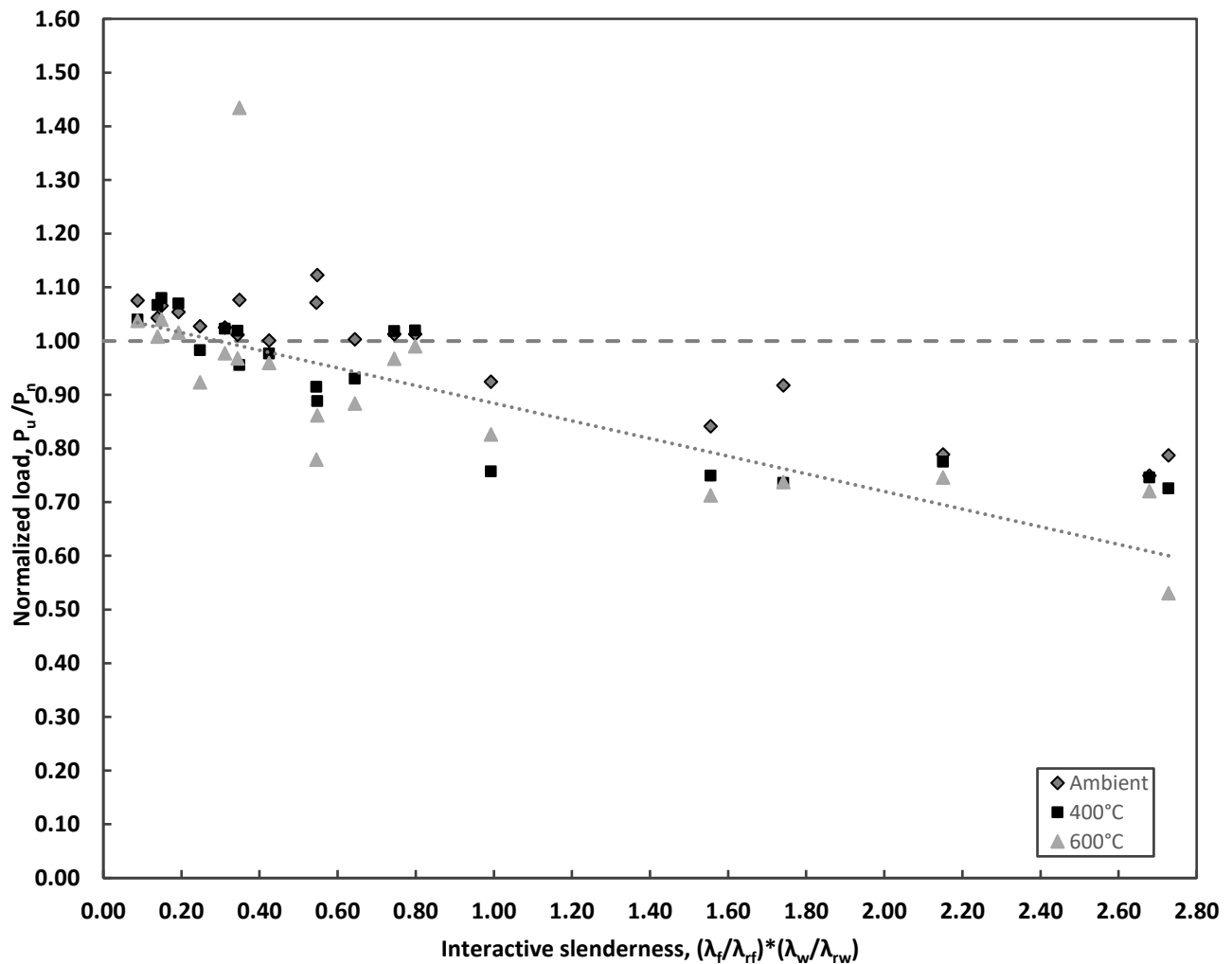


Figure 7:  $P_u/P_n$  vs interactive slenderness using AISC E7 equations for local buckling

As the interactive slenderness increases, the normalized load value decreased from 1 to 0.53. W12-H (slenderness = 0.4) and W12-J (slenderness = 1) are outliers. W12-H at 600°C is overpredicted by AISC and is predicted even greater than the capacity at ambient and 400°C. Furthermore, the capacity of W12-J at 600°C is also more than at 400°C.

## 6. Conclusions

Three different steel cross-sections were studied: W14×120, W12×96, and W10×88. These sections are not slender at ambient temperature, but W14×120 and W12×96 became slender at elevated temperature and exhibited local buckling failure modes. The columns with increased slenderness ratio were most affected at 600°C. Columns with high slenderness did not fully yield the cross-section and instead failed from local buckling. Columns with lower slenderness than the original AISC sections of W14×120, W12×96, and W10×88 failed through global buckling at all three temperatures studied. As the interactive slenderness of the column increased, the AISC 360 (2016) provisions over-estimated the column capacity at 400°C and 600°C. It was found that the current AISC equations are inadequate to accurately predict the local buckling capacity of slender columns at elevated temperature. An equation to better predict this local buckling capacity must be developed and will be part of ongoing efforts.

## References

- AISC. (2016). “*Specification for Structural Steel Buildings (ANSI/AISC 360-16)*.” American Institute of Steel Construction. Chicago, IL.
- Akhtar, M. F., & Chicchi, R. A. (2021). “Numerical investigation of the flexural buckling of high strength steel wide flange columns.” *Proceedings of the Annual Stability Conference Structural Stability Research Council 2021, SSRC 2021*, 1–12.
- British Standards Institution. (2005). “*Eurocode 3: Design of steel structures - Part 1-2: General rules - Structural fire design*.” BSI. London.
- Chen, J., & Young, B. (2008). “Design of high strength steel columns at elevated temperatures.” *Journal of Constructional Steel Research*, 64(6), 689–703.
- Seif, M., & McAllister, T. (2013). “Stability of wide flange structural steel columns at elevated temperatures.” *Journal of Constructional Steel Research*, 84, 17–26.
- Wang, W., Kodur, V., Yang, X., & Li, G. (2014). “Experimental study on local buckling of axially compressed steel stub columns at elevated temperatures.” *Thin-Walled Structures*, 82, 33–45.
- Yang, K. C., Lee, H. H., & Chan, O. (2006). “Performance of steel H columns loaded under uniform temperature.” *Journal of Constructional Steel Research*, 62(3), 262–270.